IEEE Access
Multidisciplinary | Rapid Review | Open Access Journal

Received March 16, 2021, accepted March 25, 2021, date of publication March 31, 2021, date of current version April 9, 2021.

Digital Object Identifier 10.1109/ACCESS.2021.3070048

Linear Active Disturbance Rejection Control for Double-Pendulum Overhead Cranes

LIN CHAI, QIHANG GUO, (Graduate Student Member, IEEE), HUIKANG LIU, AND MINGBO DING

College of Information Science and Engineering, Wuhan University of Science and Technology, Wuhan 430081, China

Corresponding author: Lin Chai (235126698@qq.com)

This work was supported by the National Key Research and Development Program of China under Grant 2017YFC0805100.

ABSTRACT Because of the complexity, non-linearity, and under-actuated features of double pendulum overhead cranes, a control method based on linear active disturbance rejection control (LADRC) and differential flatness theory is proposed to realize accurate trolley positioning and effective swing eliminating. Specifically, in order to simplify the system model, we introduce the differential flatness theory to construct system output. Based on this method, the uncertainty and system external disturbance become total disturbance. The control method of the crane is designed according to LADRC. Then, we use the bird swarm algorithm (BSA) to optimize controller's parameters. Finally, the double-pendulum crane control method based on the LADRC can better accomplish the crane's anti-swing and location in the real environment according to simulation and experimental results, which confirms its effectiveness and robustness in existing system.

INDEX TERMS Under-actuated crane, double-pendulum, anti-swing, tracking control, LADRC.

I. INTRODUCTION

The crane is one of the most critical components of construction machinery. The main purpose of crane control is rapidly and precisely transporting the goods to the target location without residual tipping. The control dimensionality of the crane system is less than the degrees of freedom to be controlled, which is a typical under-actuated mechatronic system. Overhead cranes are susceptible to external disturbances such as friction and wind during operation, and the system status shows non-linear and robust coupling. Many researchers have done a great deal of work to eliminate the crane's swing and positioning, and they have put forward many feasible control methods to eliminate the crane swing [1]–[14].

However, most existing control methods only take the single-stage swing characteristics of the crane system into consideration, whereas in many cases: (1) the mass between hock with load is similar which cannot ignore the hook's quality; (2) when the mass distribution of the object is uneven, and the size is too large to be regarded as a mass point. The crane system will exhibit a secondary swing characteristic that the load will swing around the hook, resulting in a more complex dynamic model of the crane system. Specifically, coupling and under-driving of double-pendulum overhead crane system are higher than single-pendulum crane, which brings significant challenges to the design of the system's anti-swing and positioning control method. Therefore, the existing single-pendulum-based crane control methods cannot achieve good performance when directly apply to the double-pendulum overhead crane system. At present, some scholars have put forward some more effective control methods for the crane with double-pendulum [15]–[39]. A control method based on path planning offers a good capability to position a trolley and eliminate the undesired oscillation in [15], [16]. In [17]–[19], sliding mode control was introduced to achieve high tracking performance and preserve strong robustness. The energy-based controllers claimed to be useful in particular conditions are developed in [20]–[24]. A control method by combining a ZV input shaper with a POS-based PID controller for a three-dimensional (3D) overhead crane is presented in [25]. A hybrid control approach, which is a combination of an offline optimal motion trajectory and a non-linear feedback controller for under-actuated overhead crane, is developed in [26]. Adaptive repetitive learning control for an offshore boom crane is proposed in [27], [28]. An optimal discrete-time command generation method is

The associate editor coordinating the review of this manuscript and approving it for publication was Kan Liu.

presented in [29]. An online trajectory generation approach for achieving both load sway reduction and cart positioning simultaneously in overhead cranes is shown in [30]. A robust two-degrees-of freedom control approach to deal with the trade-off problems between precise boom positioning and load sway suppression in a rotary crane is presented in [31]. A model predictive controller to achieve both load sway suppression and energy saving control in an overhead crane system is presented in [32]. An improved damping anti-swing signal was introduced to suppress the load sway angle in an overhead crane system [33]. An adaptive anti-swing control solution for under-actuated cranes is proposed in [34]–[37]. A new control strategy for a class of underactuated systems is proposed in [38]. An effective output feedback control method is designed for 5-DOF offshore cranes without any linearization [39]. For actuator deadzones and unavailable velocities in double pendulum overhead cranes, intelligent algorithms and quasi-velocities provide some effective solutions in [40], [41]. Linear active disturbance rejection control (LADRC) is proposed by Prof. Han Jingqing which is originated from the idea: that any control system can be transformed into a series integral standard type through feedback [42], [43]. LADRC solves many control problems by its good immunity and stable static performance [44]–[50].

In particular applications, such as high-temperature molten metal transportation, the control system needs to meet the following objectives:

1) The maximum swing angle should be strict limited and be as small as possible.
2) The control algorithm should be applicable to the harsh industrial environment.
3) The proposed algorithm should be with high reliability, high stability, and strong anti-interference ability.

However, in the recently published papers, the existing control methods cannot meet the above three goals at the same time. Hence, a control system with an active disturbance rejection controller is proposed in this paper.

For this purpose, the non-linear dynamics of the crane should be transformed into a new system that is similar to the 'single input single output system' for controller design. Then, a control system based on differential flatness [51] and LADRC is proposed for improving the precise positioning and anti-swing performance of the crane system. The stability of the whole system is verified by calculating eigenvalues of the state equation, which should meet all eigenvalues have negative real parts [52]. Combined experiments with comparative simulation, the effectiveness of the proposed control algorithm are verified.

The main contributions of this paper are concluded as follows:

1) This method converts the non-linear system into an approximate SISO system so that the maximum swing angle of the crane is within 1 degree during the whole working process.
2) The proposed algorithm can be implemented on a PLC control platform to adapt to the industrial environment.
3) Through a small crane experiment platform and comparative simulation, it is not only verified that the control method feasibility and effectiveness but also proved that the new control algorithm meets the requirements of high reliability, high stability, and strong anti-interference ability.

The rest of this paper is organized as follows: in section II, the crane model and control system is introduced. In section III, an under-actuated double-pendulum bridge crane control method and a LADRC parameter optimization method based on bird swarm algorithm (BSA) are proposed. In section IV, a series of simulations based on the proposed method, which is compared with the previous control methods, verify the proposed method's control performance. In section V, a small crane experiment platform based on Siemens S7-1200 PLC is established to realize the control algorithm based on differential flatness and LADRC. It not only verifies the control method feasibility and effectiveness but also proves that the new control algorithm is easy for engineering implementation. Finally, the section VI concludes and summarizes the contribution of the work done in this paper.

II. CRANE MODEL AND CONTROL SYSTEM

A. DOUBLE-PENDULUM OVERHEAD CRANE MODEL

Most of the existing crane modeling process omit the influence of the friction on the trolley, but the friction is common in the trolley's actual operation process. Therefore, to further improve the model's accuracy, this paper will establish the dynamic model of the general crane system based on the friction on the trolley for the crane's horizontal transportation process. Fig.1. depicts the overhead crane model, in which the dynamic model can be described by (1), as shown at the bottom of the next page.

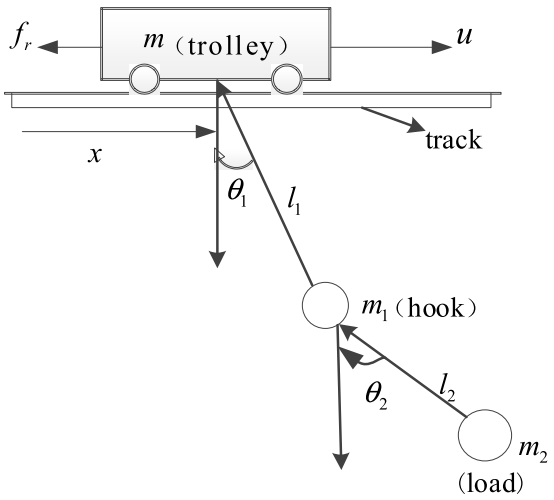

FIGURE 1. Model diagram of double-pendulum crane.

Among them:
m - trolley mass (kg);

m_1 - hook mass (kg);
m_2 - load mass (kg);
g - gravity acceleration (N/kg);
x - trolley displacement (m);
l_1 - rope length from hook to trolley (m);
l_2- rope length from hook to load (m);
u - trolley driving force (N);
f_r - trolley friction Force (N);
θ_1- the first swing angle (rad);
θ_2- the second swing angle (rad);

B. FLAT ATTRIBUTE DETERMINATION

In the crane working process, swing with a high magnitude of load can bring safety risks and reduce the system working efficiently. In practice, the maximum swing angle of the double-pendulum crane $\theta_{1\max}$ and $\theta_{2\max}$ should be kept within 10°. Their derivatives $\dot{\theta}_{1\max}, \dot{\theta}_{2\max}$ should also be limited in a small range.

Under this basis,

$$\begin{aligned} &\cos\theta_i \approx 1, \quad \cos(\theta_1-\theta_2)\approx 1, \sin\theta_i=\theta_i,\\ &\sin(\theta_1-\theta_2)\dot{\theta}_i^2 \approx 0, \quad i=1,2\\ &\sin(\theta_1-\theta_2)\dot{\theta}_i^2 \approx 0, \quad i=1,2 \end{aligned}$$

(The following control method ensures that the system two-stage swing and angular velocity remain within the above range)

Rewrite the system dynamic model as follows:

$$\begin{cases} (m+m_1+m_2)\ddot{x}+(m_1+m_2)l_1(\ddot{\theta}_1-\dot{\theta}_1^2\theta_1)\\ \quad +m_2l_2\ddot{\theta}_2-m_2l_2\dot{\theta}_2^2\theta_2=u\\ (m_1+m_2)l_1\ddot{x}+(m_1+m_2)l_1^2\ddot{\theta}_1+m_2l_1l_2\ddot{\theta}_2\\ \quad +(m_1+m_2)gl_1\theta_1=0\\ m_2l_2\ddot{x}+m_2l_1l_2\ddot{\theta}_1+m_2l_2^2\ddot{\theta}_2+m_2gl_2\theta_2=0 \end{cases} \tag{2}$$

The 2nd and 3rd equations in the system model described by (2) can be transformed as follows:

$$\ddot{x}+l_1\ddot{\theta}_1+\frac{m_2l_2}{m_1+m_2}\ddot{\theta}_2+g\theta_1=0 \tag{3}$$

$$\ddot{x}+l_1\ddot{\theta}_1+l_2\ddot{\theta}_2+g\theta_2=0 \tag{4}$$

Supposing the horizontal displacement signal of the load being x_z, it can be obtained that

$$x_z=x+l_1\theta_1+l_2\theta_2 \tag{5}$$

Combining (4) with (5), we can get

$$\theta_2=-\frac{\ddot{x}_z}{g} \tag{6}$$

From (6), it can be derived that

$$\dot{\theta}_2=-\frac{x_z^{(3)}}{g} \tag{7}$$

$$\ddot{\theta}_2=-\frac{x_z^{(4)}}{g} \tag{8}$$

Substitute (7) and (8) into (3) and (4), we can get

$$\theta_1=-\frac{\ddot{x}_z}{g}-\frac{m_1l_2}{(m_1+m_2)\,g^2}x_z^{(4)} \tag{9}$$

$$\dot{\theta}_1=-\frac{x_z^{(3)}}{g}-\frac{m_1l_2}{(m_1+m_2)\,g^2}x_z^{(5)} \tag{10}$$

$$\ddot{\theta}_1=-\frac{x_z^{(4)}}{g}-\frac{m_1l_2}{(m_1+m_2)\,g^2}x_z^{(6)} \tag{11}$$

Substitute (6) and (9) into (5), horizontal displacement x can be obtained as follows:

$$x=x_z+\frac{(l_1+l_2)}{g}\ddot{x}_z+\frac{m_1l_1l_2}{(m_1+m_2)\,g^2}x_z^{(4)} \tag{12}$$

From (12), it can be derived that

$$x^{(i)}=x_z^{(i)}+\frac{l_1+l_2}{g}x_z^{(i+2)}+\frac{m_1l_1l_2}{(m_1+m_2)\,g^2}x_z^{(i+4)} \tag{13}$$

Thus, all system states can be expressed in the algebra and form of its different order derivatives from the above. Therefore, the output of the crane kinematics system is differentially flat. At this time, the system (13) is similar to the 'single input single output system', which indicates that the system has no under-driving characteristics.

C. LINEAR ACTIVE DISTURBANCE REJECTION CONTROL SYSTEM

The LADRC is originated from the idea: that any control system can be transformed into a series integral standard type through feedback [52]–[54]. Most objects can be described as follows:

$$\begin{cases} x^{(n)}=f(x,\dot{x},\ldots x^{(n-1)},x^{(n)},w(t),u,\dot{u},\ldots,u^{(n)},t)+bu\\ y=x(t) \end{cases} \tag{14}$$

In (14), $w(t)$ represents unknown external disturbance; u represents input; n is the system order; b is the control gain; y is the system output; $x, \dot{x}, \ldots\ldots, x^{(n-1)}, x^{(n)}$ represent the system state quantity and the n-order derivative of the state quantity; the $f(x,\dot{x},\ldots x^{(n-1)},x^{(n)},w(t),u,\dot{u},\cdots,u^{(n)},t)$ related to the unknown external disturbance represents real-time action, the system state, and its derivatives are classified as the

$$\begin{cases} (m+m_1+m_2)\ddot{x}+(m_1+m_2)l_1(cos\theta_1\ddot{\theta}_1-\dot{\theta}_1^2sin\theta_1)+m_2l_2\ddot{\theta}_2cos\theta_2-m_2l_2\dot{\theta}_2^2sin\theta_2=u-f_r\\ (m_1+m_2)l_1cos\theta_1\ddot{x}+(m_1+m_2)l_1^2\ddot{\theta}_1+m_2l_1l_2\cos(\theta_1-\theta_2)\ddot{\theta}_2+m_2l_1l_2\sin(\theta_1-\theta_2)\dot{\theta}_2^2+(m_1+m_2)gl_1\sin\theta_1=0\\ m_2l_2cos\theta_2\ddot{x}+m_2l_1l_2\cos(\theta_1-\theta_2)\ddot{\theta}_1+m_2l_2^2\ddot{\theta}_2-m_2l_1l_2\sin(\theta_1-\theta_2)\dot{\theta}_1^2+m_2gl_2\sin\theta_2=0 \end{cases} \tag{1}$$

total disturbance. To simplify the description, we abbreviate it as f. Then an expansion state $x_1, x_2, \cdots, x_{n+1}$ satisfy:

$$\begin{cases} \dot{x}_1 = x_2 \\ \dot{x}_2 = x_3 \\ \vdots \\ \dot{x}_{n-1} = x_n \\ \dot{x}_n = f(X, \omega) + bu \\ y = x_1 \end{cases} \tag{15}$$

Among them, $X = [x_1, x_2, \cdots, x_{n+1}]^{\mathrm{T}}$, e is observation error. A linear extended state observer (LESO) can be established as follows:

$$\begin{cases} e = z_1 - y_1 \\ \dot{z}_1 = z_2 - \beta_1 e \\ \dot{z}_2 = z_3 - \beta_2 e \\ \vdots \\ \dot{z}_{n-1} = z_n - \beta_{n-1} e \\ \dot{z}_n = -\beta_n e + bu \end{cases} \tag{16}$$

Among them, z_i is the estimated value of $x_z^{(i-1)}$. β_i is the observer gain coefficient.

When the dynamic model of the controlled object (14) is known, the above is a known function, and its derivative $\dot{f}$ is also fully known, then its state can be described as (15).

Introducing the matrix

$$A = \begin{bmatrix} 0 & 1 & 0 & \cdots & 0 \\ 0 & 0 & 1 & \cdots & 0 \\ 0 & 0 & 0 & \cdots & 0 \\ 0 & 0 & 0 & \cdots & 1 \\ 0 & 0 & 0 & \cdots & 0 \end{bmatrix}$$
$$B = \begin{bmatrix} 0 & \cdots & 0 & b & 0 \end{bmatrix}^{\mathrm{T}}$$
$$X = [x_1, x_2, \cdots, x_{n+1}]^{\mathrm{T}}$$

Then, the (15) can be expressed as

$$\dot{X} = AX + Bu \tag{17}$$

D. STABILITY ANALYSIS

For the convenience of analysis, we denote the observation value corresponding to $x_i (i = 1, 2, L, n+1)$ as $\tilde{x}_i (i = 1, 2, L, n+1)$.

$$\dot{\tilde{X}} = A\tilde{X} + Bu + L(X - \tilde{X}) \tag{18}$$

Among them, A is the observation vector of the expanded observer. B is the gain constant matrix of the optional observer:

$$L = \begin{bmatrix} l_1 & 0 & \cdots & 0 \\ l_2 & 0 & \cdots & 0 \\ \vdots & \vdots & \ddots & \vdots \\ l_{n+1} & 0 & \cdots & 0 \end{bmatrix}_{(n+1)\times(n+1)} \tag{19}$$

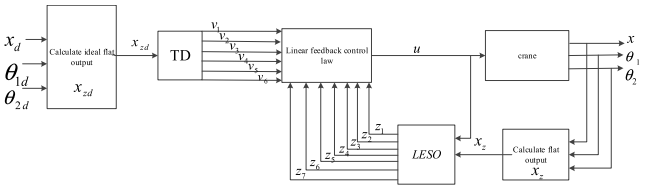

FIGURE 2. Control block of differential flatness and LADRC.

Subtract (18) from (17):

$$\dot{X} - \dot{\tilde{X}} = (A - L)(X - \tilde{X}) \tag{20}$$

In order to make the estimation error approaches zero, the matrix must satisfy the Hurwitz criterion. That is, its eigenvalues have negative real parts.

So, we can get the following theorem:

Theorem 1: For a linear time-invariant system, $\begin{cases} \dot{x} = Ax + bu \\ y = Cx \end{cases}$, and the equilibrium state $x_e = 0$ is asymptotically stable. The necessary and sufficient condition is that all eigenvalues of the matrix have negative real parts.

The core idea of LADRC is to estimate the system's total disturbance $f(x, \dot{x}, ...x^{(n-1)}, x^{(n)}, w(t), u, \dot{u}, \cdots, u^{(n)}, t)$ reasonably and compensate the system to offset the total disturbance at the source, and then the system becomes a integral series type. The design of a suitable control rate for the series integral system makes the system easier to implement.

The premise of the above design only needs to require the total disturbance to be bounded. Whether it is time-varying linear or non-linear, known or unknown, is not essential. The LADRC essentially linearizes the main parameters of the active disturbance rejection so that when the system reaches the same performance index, the undetermined parameters are reduced, and the parameter setting is more uncomplicated.

III. DESIGN OF LARDC METHOD FOR UNDER-ACTUATED DOUBLE-PENDULUM OVERHEAD CRANE

In section II, the linear active disturbance rejection system's stability condition is analyzed, namely Theorem 1. Then an under-actuated double-pendulum bridge crane active disturbance rejection control method is designed.

A. CONTROLLER STRUCTURE

In Fig.2., x_d, θ_{1d} and θ_{2d} are the expected value of the trolley displacement, load first swing angle, and load second swing angle, respectively; x, θ_1, θ_2 is the actual output displacement of the trolley, the swing angle of the first load, and the second swing angle respectively; x_{zd}, x_z is the expected value of the system flat output and the actual value of the flat output respectively; $v_i (i = 1, 2, 3, 4, 5, 6)$ is the transition process of the expected flat output and its 1, 2, 3, 4, and 5 derivatives respectively; $z_i (i = 1, 2, 3, 4, 5, 6)$ is the estimated value of the actual flat output and its 1, 2, 3, 4, and 5 derivatives respectively; z_7 is the estimated value of system's total disturbance.

Substitute the (6)-(13) into 1st in the system model described by (2), and (21), as shown at the bottom of the page, is obtained.

Transform the (21) into the following form, which is shown in (22):

$$\begin{cases} \dot{x}_1 = x_2 \\ \dot{x}_2 = x_3 \\ \dot{x}_3 = x_4 \\ \dot{x}_4 = x_5 \\ \dot{x}_5 = x_6 \\ \dot{x}_6 = f_1(x_3, x_4, x_5, x_6) + bu \end{cases} \tag{22}$$

Specifically, it can be defined that

$x_1 = x_z, x_2 = x_z', x_3 = x_z^{(2)}, x_4 = x_z^{(3)}, x_5 = x_z^{(4)}, x_6 = x_z^{(5)}$.

In particular, $f_1(\mathrm{x}_3, \mathrm{x}_4, \mathrm{x}_5, \mathrm{x}_6)$ and b can be depicted as (23), shown at the bottom of the page.

Supposing that b_0 is the estimated value of b, (22) can be rewritten as (24).

$$\begin{cases} \dot{x}_1 = x_2 \\ \dot{x}_2 = x_3 \\ \dot{x}_3 = x_4 \\ \dot{x}_4 = x_5 \\ \dot{x}_5 = x_6 \\ \dot{x}_6 = f(x_3, x_4, x_5, x_6) + b_0 u \end{cases} \tag{24}$$

Among them

$$f(x_3, x_4, x_5, x_6) = f_1(x_3, x_4, x_5, x_6) + (b - b_0)u$$

The total disturbance of the system is f.

B. CONTROLLER DESIGN

(1) Design a Tracking Differentiator (TD)for the crane system intended flat input x_{zd}. According to (5):

$$x_{zd} = x_d + l_1\theta_{1d} + l_2\theta_{2d} \tag{25}$$

In (25), x_d is crane intended horizontal displacement; θ_{1d} and is the first-stage oscillation angle expected by the system, θ_{2d} is the second-stage swing angle expected by the system, and both θ_{1d} and θ_{2d} are set to 0; therefore, (25) can be further simplified to:

$$x_{zd} = x_d \tag{26}$$

Therefore, we can immediately determine the input of the TD. The TD is designed as follows:

$$\begin{cases} \dot{v}_1 = v_2 \\ \dot{v}_2 = v_3 \\ \dot{v}_3 = v_4 \\ \dot{v}_4 = v_5 \\ \dot{v}_5 = v_6 \\ \dot{v}_6 = -r(r(r(r(r(v_1 - v_0) + 6v_2) + 15v_3) \\ \qquad +20v_4) + 15v_5) + 6v_6) \end{cases} \tag{27}$$

In (27), v_0 is displacement command setting value, $v_0 = x_{zd}$, and v_1 in this system is the transition process arranged by TD; v_2 is the approximate differential of v_1; v_3 is the approximate second derivative of v_1; v_4 is the approximate third derivative of v_1; v_5 is the approximate fourth derivative of v_1; v_6 is the approximate fifth derivative of v_1; r is a parameter used to adjust the differential tracker performance, which can be adjusted according to system requirements

2) For system flat output, a LESO is designed as follows:

$$\begin{cases} e = z_1 - x_d \\ \dot{z}_1 = z_2 - \beta_1 e \\ \dot{z}_2 = z_3 - \beta_2 e \\ \dot{z}_3 = z_4 - \beta_3 e \\ \dot{z}_4 = z_5 - \beta_4 e \\ \dot{z}_5 = z_6 - \beta_5 e \\ \dot{z}_6 = z_7 - \beta_6 e + b_0 u \\ \dot{z}_7 = -\beta_7 e \end{cases} \tag{28}$$

$$\begin{aligned} & x_z^{(6)} + \frac{m_1 l_2 x^{(2)} x_z^{(5)^2}}{mg^3} + \frac{m_1^2 l_2^2 x_z^{(4)} x_z^{(5)^2}}{m(m_1+m_2)g^4} + \frac{2(m_1+m_2)x_z^{(2)} x_z^{(3)} x_z^{(5)}}{mg^2} + \frac{2m_1 l_2 x_z^{(3)} x_z^{(4)} x_z^{(5)}}{mg^3} + \frac{(m_1+m_2)x_z^{(3)^2} x_z^{(4)}}{mg^2} \\ & + \left[\frac{m(m_1+m_2)l_1 g + (m+m_1)(m_1+m_2)l_2 g}{mm_1 l_1 l_2}\right] x_z^{(4)} + \left[\frac{(m_1+m_2)m_2}{mm_1 l_1 g} + \frac{(m_1+m_2)^2}{mm_1 l_2 g}\right] x_z^{(2)} x_z^{(3)^2} \\ & + \frac{(m+m_1+m_2)(m_1+m_2)g^2}{mm_1 l_1 l_2} x_z^{(2)} = \frac{(m_1+m_2)g^2}{mm_1 l_1 l_2} u \end{aligned} \tag{21}$$

$$\begin{cases} f_1(\mathrm{x}_3, \mathrm{x}_4, \mathrm{x}_5, \mathrm{x}_6) = -\dfrac{m_1 l_2 x^{(2)} x_z^{(5)^2}}{mg^3} - \dfrac{m_1^2 l_2^2 x_z^{(4)} x_z^{(5)^2}}{m(m_1+m_2)g^4} - \dfrac{2(m_1+m_2)x_z^{(2)} x_z^{(3)} x_z^{(5)}}{mg^2} - \dfrac{2m_1 l_2 x_z^{(3)} x_z^{(4)} x_z^{(5)}}{mg^3} \\ -\dfrac{(m_1+m_2)x_z^{(3)^2} x_z^{(4)}}{mg^2} - \left[\dfrac{m(m_1+m_2)l_1 g + (m+m_1)(m_1+m_2)l_2 g}{mm_1 l_1 l_2}\right] x_z^{(4)} - \left[\dfrac{(m_1+m_2)m_2}{mm_1 l_1 g} + \dfrac{(m_1+m_2)^2}{mm_1 l_2 g}\right] x_z^{(2)} x_z^{(3)^2} \\ -\dfrac{(m+m_1+m_2)(m_1+m_2)g^2}{mm_1 l_1 l_2} x_z^{(2)} b = \dfrac{(m_1+m_2)g^2}{mm_1 l_1 l_2} \end{cases} \tag{23}$$

where $z_1, z_2, z_3, z_4, z_5, z_6, z_7$ is the estimated value of output x_z, x_z', x_z'' $x_z^{(3)}$, $x_z^{(4)}$, $x_z^{(5)}$, $x_z^{(6)}$ and the estimated value of f, separately. The b_0 is b's estimated value in (28). $\beta_1, \beta_2, \beta_3, \beta_4, \beta_5, \beta_6, \beta_7$ are the observer gain coefficient. To set up the observer's seven closed-loop poles to ensure stability, they satisfy the following relation:

$$s^7 + \beta_1 s^6 + \beta_2 s^5 + \beta_3 s^4 + \beta_4 s^3 + \beta_5 s^2 + \beta_6 s + \beta_7 = (s + \omega_o)^7 \quad (29)$$

Therefore, the following mathematical relationship can be concluded:

$$\begin{cases} \beta_1 = 7\omega_o \\ \beta_2 = 21\omega_o^2 \\ \beta_3 = 35\omega_o^3 \\ \beta_4 = 35\omega_o^4 \\ \beta_5 = 21\omega_o^5 \\ \beta_6 = 7\omega_o^6 \\ \beta_7 = \omega_o^7 \end{cases} \quad (30)$$

ω_0 is observer bandwidth.

PD control law can be designed as follows:

$$\begin{cases} e_1 = v_1 - z_1 \\ e_2 = v_2 - z_2 \\ e_3 = v_3 - z_3 \\ e_4 = v_4 - z_4 \\ e_5 = v_5 - z_5 \\ e_6 = v_6 - z_6 \\ u_0 = \alpha_1 e_1 + \alpha_2 e_2 + \alpha_3 e_3 + \alpha_4 e_4 + \alpha_5 e_5 + \alpha_6 e_6 \\ u = u_0 - \dfrac{z_7}{b_0} \end{cases} \quad (31)$$

Among them, u_0 is system PD control law; u is controller actual output; $\alpha_1, \alpha_2, \alpha_3, \alpha_4, \alpha_5$, and α_6 is the controller's gain coefficient. For the sake of configuring the six closed-loop poles of the system at $-\omega_c$, there is the following relationship:

$$s^6 + \alpha_1 s^5 + \alpha_2 s^4 + \alpha_3 s^3 + \alpha_4 s^2 + \alpha_5 s + \alpha_6 = (s + \omega_c)^6 \quad (32)$$

Therefore:

$$\begin{aligned} \alpha_1 &= 6\omega_c, \quad \alpha_2 = 15\omega_c^2, \ \alpha_3 = 20\omega_c^3, \\ \alpha_4 &= 15\omega_c^4, \quad \alpha_5 = 6\omega_c^5, \ \alpha_6 = \omega_c^6 \end{aligned} \quad (33)$$

Among them, ω_c is controller bandwidth.

By adjusting ω_c and ω_o, we can find the appropriate controller and observer for crane system.

C. CONTROLLER PARAMETER OPTIMIZATION

Because of the coupling between ω_c with ω_o, and uncertain debugging rules for the agreement of LADRC controller settings, it is still challenging to tune its parameters. By studying intelligent optimization algorithms in crane control, bird swarm algorithm (BSA) [56]–[58] is introduced to optimize

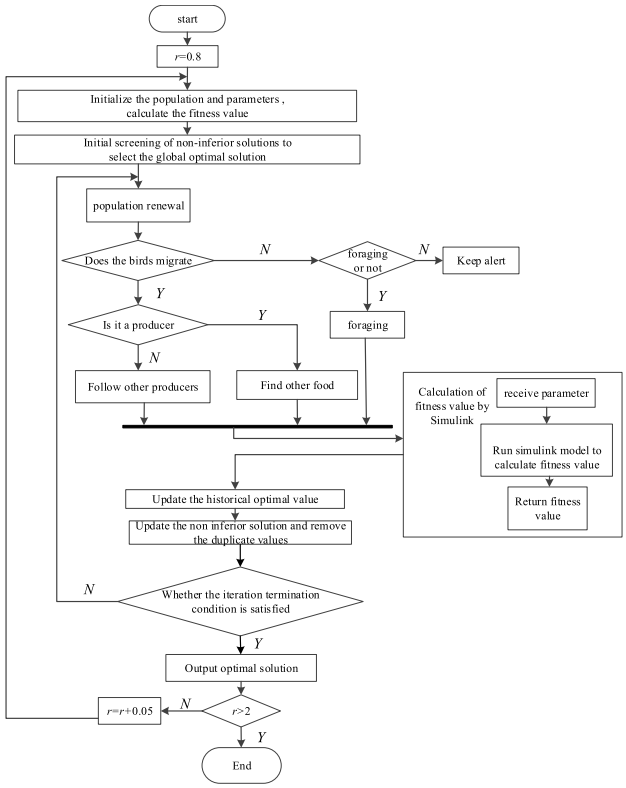

FIGURE 3. BSA optimization flow chart.

LADRC parameters. BSA has good global optimization ability, which can avoid the local optimization point and get a better global solution.

According to [59], considering system requirements, r can be limited to 0.8-2, which step size is 0.05. The ω_c and ω_o are correspond with each of r. Finally, the optimal control parameters of all-around performance are obtained.

Combined MATLAB with Simulink, the designed system parameter can be optimized by offline optimization algorithm. Among them, MATLAB is used for the r-parameter trial-and-error by BSA function, Simulink is used to construct the crane system and calculate the fitness function. The optimization flow of the algorithm is shown in Fig.3.

In this system, the dimension of each bird BSA position is 2. The BSA position represents bandwidth ω_c and observer bandwidth ω_o, respectively.

Combining (25) and (27), the fitness function of the system is shown in (34).

$$\begin{cases} x_z = x + l_1\theta_1 + l_2\theta_2 \\ x_{zd} \approx v_1 \\ e(t) = x_{zd} - x_z \\ fitness = \int_0^T t\,|e(t)|\,dt \end{cases} \quad (34)$$

Considering that the existing system bandwidth cannot be zero or very large, the upper limit of each dimension of the variable is 300, and the lower limit is 0.001. Evolution algebra

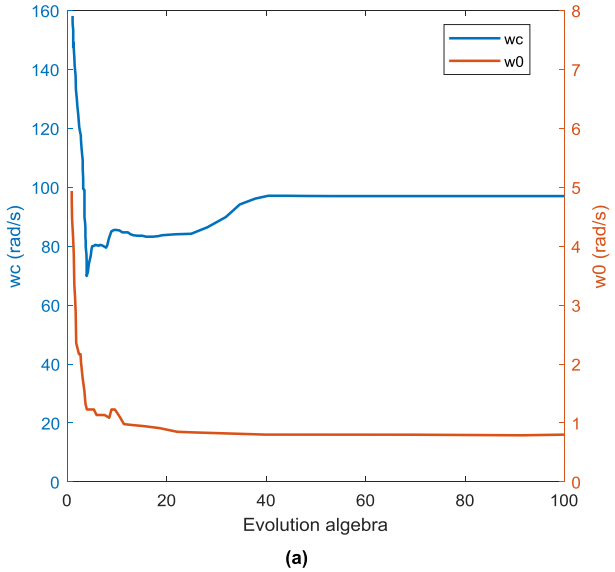

(a)

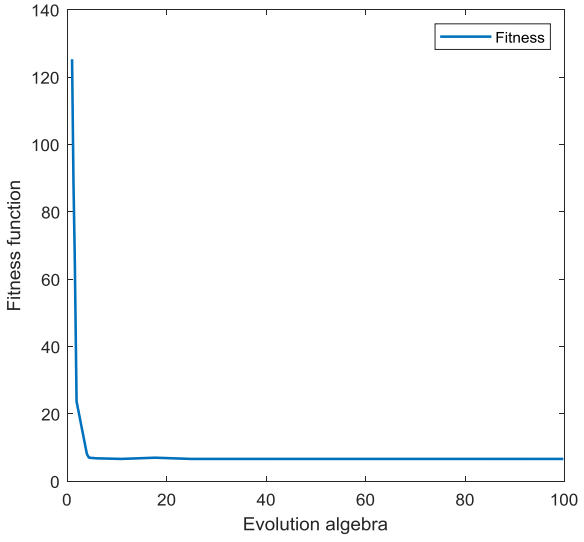

(b)

FIGURE 4. (a) Controller parameter curve and (b) fitness curve.

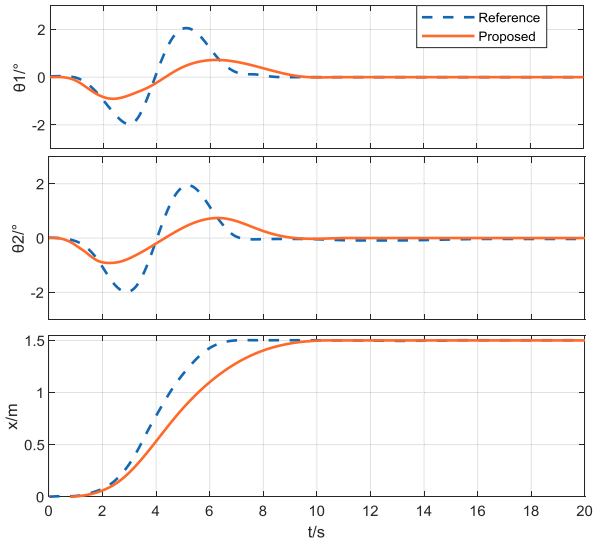

FIGURE 5. Tolley displacement and swing angle.

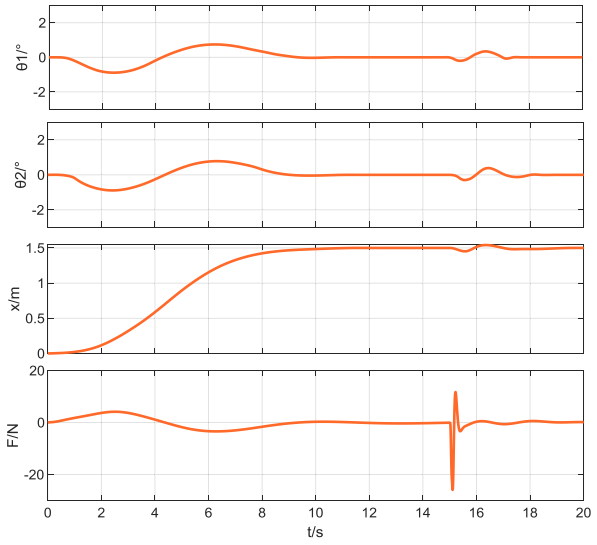

FIGURE 6. Results of anti-interference simulation.

TABLE 1. System simulation model parameters.

m[kg]	20	m_2[kg]	5	l_2[m]	0.2	x_d[m]	1.5
m_1[kg]	5	l_1[m]	2	g[m/s^2]	9.8	-	-

is 100, population size is 30, cognitive coefficient is $C_1 = C_2 = 1.5$, acceleration coefficient is $A_1 = A_2 = 1$, foraging cycle is $F_q = 3$. The whole offline parameter optimization process initializes BSA main function, then transfers the parameters to the system Simulink model through the assigning function. After running the simulation time T, the Simulink model fitness function value will be returned to the main function. BSA main function updates the parameters according to the fitness function value and starts from cycle to cycle until the last generation. The optimization result of the algorithm is shown in Fig.4.

After the offline operation optimization algorithm is completed, the parameter r of TD can be updated. Afterwards, the bird swarm algorithm will calculate 3000 times in the computer, and the controller optimal parameters corresponding to r can be obtained. Considering the lifting efficiency and anti-swing effect of the system, the optimal controller parameters are obtained as: $r = 1.25, \omega_o = 97, \omega_c = 0.8$.

IV. SIMULATION RESULTS AND ANALYSIS

To verify the controller control effectiveness, a simulation is conducted through Simulink environment. TABLE 1 shows system model parameters. In this section, the proposed method effectiveness is verified by numerical simulation and compared with the planned trajectory control method in reference [60]. The result is shown in Fig.5.

From the results in TABLE 2, the method in this paper can achieve rapid and accurate positioning of the trolley

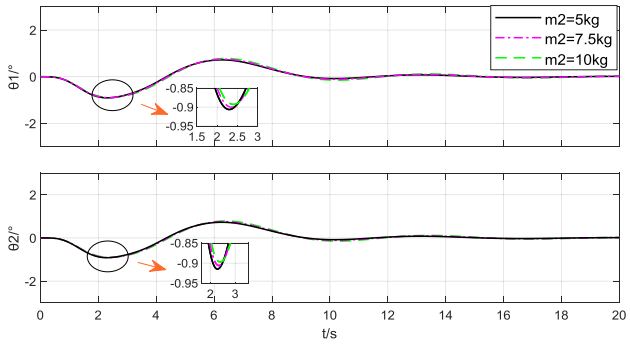

FIGURE 7. Simulation results of load mass change.

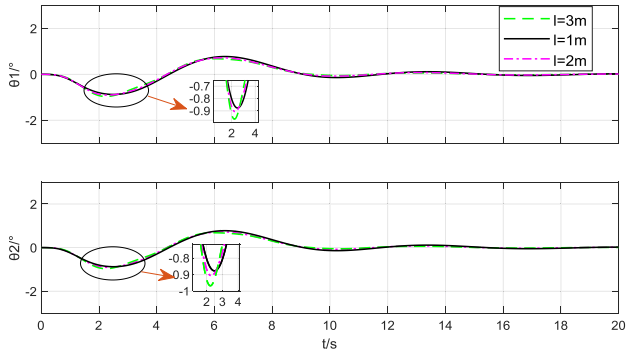

FIGURE 8. Simulation results of rope length change.

TABLE 2. Performance indices .

Control methods	$\theta_{1\max}$	$\theta_{2\max}$	θ_{res}	t_s
proposed	0.90635	0.91475	<0.1	10.7120
reference	2	2	<0.1	8.1360

under the premise that the maximum swing angle is smaller and entirely suppress and eliminate the two-stage swing of the system, which is consistent with the theoretical analysis. Although the trajectory planning control method in [60] achieves shorter transportation time, in some industrial situations with extremely strict diagonal swing angle, such as high-temperature molten metal transport, the requirements for the rapidity of transportation are relatively minor. Therefore, the control method proposed in this paper has obvious practical significance in this industrial situation with an extremely strict diagonal swing angle.

The following three sets of simulation experiments are carried out to prove the proposed controller robustness in the presence of external interference.

1) Given that the crane may be impeded by wind resistance, it is decided to apply a force of 20 N for 0.1 seconds.

2) Whereas the crane's load can change, the load mass increase from 5kg to 7.5kg and 10kg, respectively.

3) Considering the possible changes in the crane's rope length, increase or decrease the rope length by 50%. The following three series of photographs are experimental 1), 2), and 3).

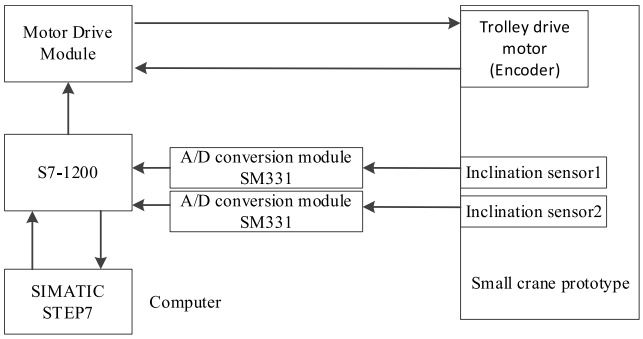

FIGURE 9. System structure diagram.

FIGURE 10. (a) Physical drawings of sensors and (b) sensor installation drawings.

In Fig.6., the system can quickly return to a steady state in 1 second when the impact force is added to the system at 15th second. External disturbance has little effect on rocking angle and crane movement. In other words: the system has a good ability to anti-interference to external disturbance.

In Fig.7., as the load mass increases, the rocking angle decreases further, and the stabilization time increases. Still, the rocking angle is quickly checked to within 1° with no residual oscillation. The system has a great anti-interference ability to load mass disturbance.

In Fig. 8., when the length of the rope is reduced by 50%, the flip angle decreases. When the length of the rope is increased by 50%, the flip angle increases slightly to 0.97°, which is less than 1°. The trolley displacement response is almost the same. In other words, the system has excellent anti-interference capacity against the change of rope length parameters.

V. EXPERIMENTS SET UP AND RESULTS

In this chapter, we design and develop a set of PLC-based system with the implementation of LADRC to verify proposed methods [55]. Firstly, the LADRC algorithm is designed by ladder programmed language in PLC, and then the parameters obtained by the simulation algorithm in section v are tested in the system platform. The experiment results verify the effectiveness and robustness of the LADRC algorithm in the existing system.

A. EXPERIMENTAL SYSTEM

The experimental verification platform of the LADRC algorithm based on PLC is designed in this paper. As shown in Fig. 9., it is to verify that the proposed strategy can achieve

FIGURE 11. Prototype crane.

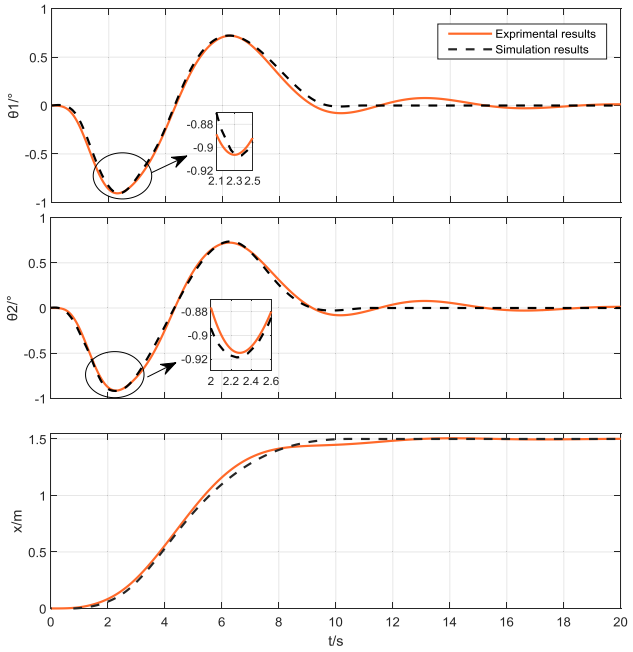

FIGURE 12. Angle results and displacement results of experiment.

the anti-swing and fast positioning of the double-pendulum crane. In other words, it proves that the proposed method is easy to implement and apply to the industrial controller. Typical crane control system hardware includes an upper computer, PLC control module, power supply module, inclination sensor, motor drive module, and small crane prototype.

The experimental platform includes Siemens S7-1200 PLC controller and motor drive module SINAMICS S120. Among them, the proposed control algorithm is implemented through Siemens S7-1200 PLC controller. The tilt angle is measured through tilt sensor RION SDA128T30-A1. The trolley displacement feedback signal and tilt sensor data are collected through TIA software. The installation of the tilt sensor is shown in Fig. 10. The whole crane system is shown in Fig. 11. The specific LADRC implementation method is presented in Appendix.

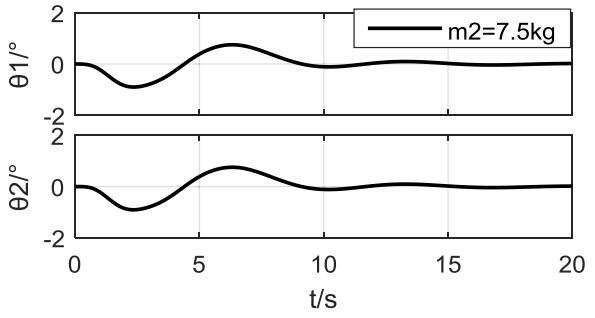

FIGURE 13. Experimental results of m2 = 7.5kg.

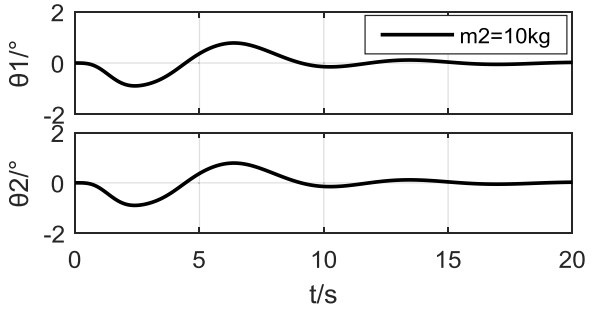

FIGURE 14. Experimental results of m2 = 10kg.

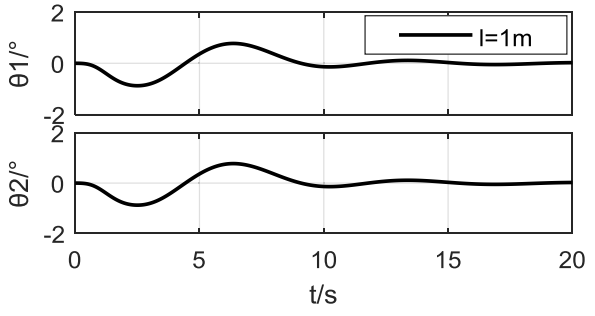

FIGURE 15. Experimental results of l = 1m.

B. EXPERIMENTAL RESULTS

The experimental load is selected as a five-kilogram weight. The trolley mechanism total weight and the load-lifting mechanism is about 20kg. The rope length is 2m. The desired displacement of the trolley is set to 1.5m, and the friction coefficient of the trolley is taken as the reference value of the data manual 0.2.

Set the TD adjusting parameter $r = 1.25$ and estimate the b of system parameter $b_0 = 0.1$. First, BSA is used to optimize the algorithm to find a set of appropriate reference values of controller parameters and then adjust them based on reference values to complete parameter tuning quickly. The controller parameters are selected as follows: $\omega_o = 97$, $\omega_c = 0.8$, $b_0 = 0.1$; through the debug curve module of the TIA software, the swing angle can be observed in real-time, and the corresponding control effect is shown in Fig.12.

The robustness of the LADRC algorithm can is shown in Fig.13., Fig.14., Fig.15., and Fig.16.

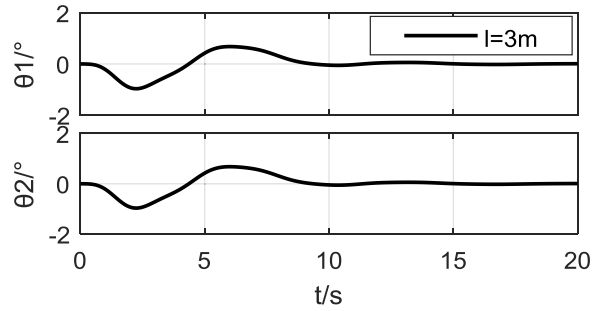

FIGURE 16. Experimental results of l = 3m.

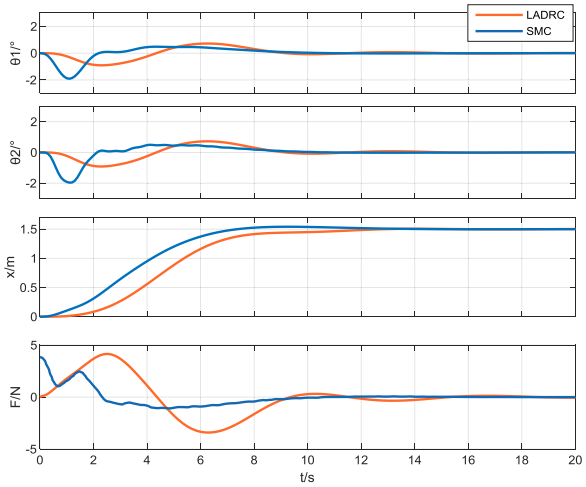

FIGURE 17. Experimental results of LARDC and SMC.

To further verify the performance of the proposed controller, a control effect comparison between LADRC with Sliding Mode Control (SMC) [17] is depicts in Fig.17.

From the results in Fig.17., the method proposed in this paper can achieve rapid and accurate positioning of the trolley under the premise that the maximum swing angle is smaller than SMC [17] and entirely suppress and eliminate the two-stage swing of the system. Therefore, the control method proposed in this paper has obvious practical significance in industrial situation with an extremely strict swing angle.

The experimental environment can simulate the industrial field. There is a large amount of noise in the signal of the sensors, the performance of the cart deceleration box is also not ideal. As the friction force experienced by the actual bench is very complex, the fixed friction coefficient cannot reflect the actual situation of friction force between crane and track. Therefore, the established model cannot fully represent the actual work of the crane. However, the experimental results show that the anti-swing and fast positioning of the double-pendulum crane can be achieved by the LADRC, which further proves the effectiveness and robustness of the control strategy proposed by this paper.

VI. CONCLUSION

LADRC theory is the first time applied to the double-pendulum crane system anti-swing and quick positioning control. Among them, the parameters of the controller are optimized by the BSA optimization algorithm. According to the simulation results, we can see that the method has an excellent performance in eliminating swing and positioning error, and has good anti-interference ability, and robust to external disturbance and changes in model parameters (quality and rope length). The experimental results show that the double pendulum crane control method based on the LADRC can accomplish the crane anti-swing and location in the industrial environment, which further confirms the effectiveness and robustness of the proposed method.

APPENDIX

Necessary algorithm procedures in Fig.2. are shown as follows:

function sys = mdlDerivatives(t,x,u,r)% r is the TD parameter
sys(1) = x(2);
sys(2) = x(3);
sys(3) = x(4);
sys(4) = x(5);
sys(5) = x(6);
sys(6) = − r*(r*(r*(r*(r*(r*(x(1) − u)+6*x(2))+15*x(3))
+20*x(4)) +15*x(5))+6*x(6));
function sys = mdlOutputs(t,x,u,wc,b0)
% wc is the controller bandwidth and b0 is the estimated value of bb
k1 = 6*wc; k2 = 15*wc^2; k3 = 20*wc^3; k4 = 15*wc^4;
k5 = 6*wc^5; k6 = wc^6;
z1 = u(1); z2 = u(2); z3 = u(3); z4 = u(4); z5 = u(5);
z6 = u(6); z7 = u(7);
v1 = u(8); v2 = u(9); v3 = u(10); v4 = u(11); v5 = u(12);
v6 = u(13);
error1 = v1-z1; error2 = v2-z2; error3 = v3-z3;
error4 = v4-z4; error5 = v5-z5;
error6 = v6-z6;
u0 = k1* error1+ k2*error2+k3*error3+k4*error4
+k5*error5+k6*error6;
uf = u0-z7/b0;
sys(1) = uf;

The specific LADRC implementation method is as follows:

1) Assuming the sampling time is h, the LADRC controller is discretized:

From (27), the TD can be discretized as

$$\begin{cases} v_1(k+1) = v_1(k) + hv_2(k) \\ v_2(k+1) = v_2(k) + hv_3(k) \\ v_3(k+1) = v_3(k) + hv_4(k) \\ v_4(k+1) = v_4(k) + hv_5(k) \\ v_5(k+1) = v_5(k) + hv_6(k) \\ v_6(k+1) = v_6(k) + h[-r(r(r(r(r(r(v_1(k) \\ \quad -v_0(k+1)) + 6v_2(k)) + 15v_3(k)) + 20v_4(k)) \\ \quad +15v_5(k)) + 6v_6(k))] \end{cases} \tag{35}$$

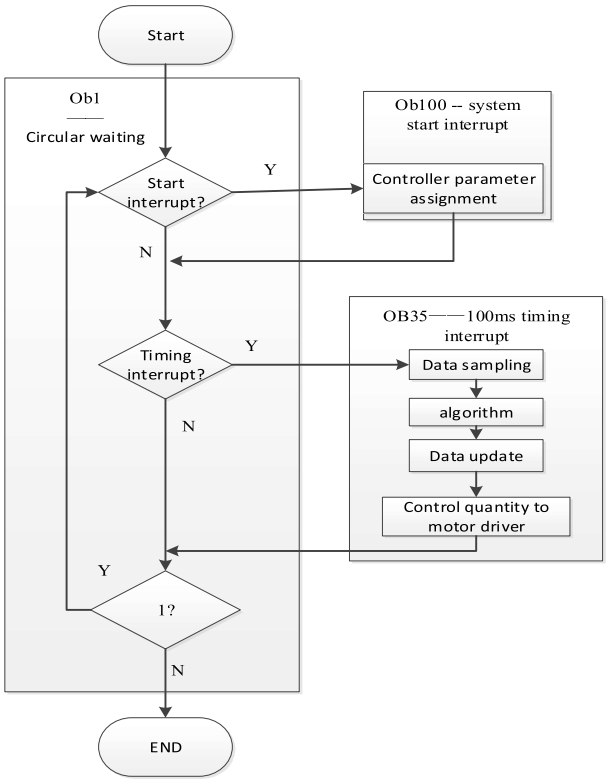

FIGURE 18. Flowchart of the PLC algorithm.

From (28)-(30), the LESO can be discretized as

$$\begin{cases} e(k+1) = z_1(k) - y(k+1) \\ z_1(k+1) = z_1(k) + h(z_2(k) - 7\omega_o e(k+1)) \\ z_2(k+1) = z_2(k) + h(z_3(k) - 21\omega_o^2 e(k+1)) \\ z_3(k+1) = z_3(k) + h(z_4(k) - 35\omega_o^3 e(k+1)) \\ z_4(k+1) = z_4(k) + h(z_5(k) - 35\omega_o^4 e(k+1)) \\ z_5(k+1) = z_5(k) + h(z_6(k) - 21\omega_o^5 e(k+1)) \\ z_6(k+1) = z_6(k) + h(z_7(k) - 7\omega_o^6 e(k+1) + b_0 u(k)) \\ z_7(k+1) = z_7(k) - h\omega_o^7 e(k+1) \end{cases} \tag{36}$$

From (31)-(33), the PD control law can be discretized as

$$\begin{cases} e_1(k+1) = v_1(k+1) - z_1(k+1) \\ e_2(k+1) = v_2(k+1) - z_2(k+1) \\ e_3(k+1) = v_3(k+1) - z_3(k+1) \\ e_4(k+1) = v_4(k+1) - z_4(k+1) \\ e_5(k+1) = v_5(k+1) - z_5(k+1) \\ e_6(k+1) = v_6(k+1) - z_6(k+1) \\ u_0(k+1) = 6\omega_c e_1(k+1) + 15\omega_c^2 e_2(k+1) \\ \qquad +20\omega_c^3 e_3(k+1) + 15\omega_c^4 e_4(k+1) + 6\omega_c^5 e_5(k+1) \\ \qquad +\omega_c^6 e_6(k+1) \\ u = u_0(k+1) - \dfrac{z_7(k+1)}{b_0} \end{cases} \tag{37}$$

2)PLC implementation of discrete LADRC controller:

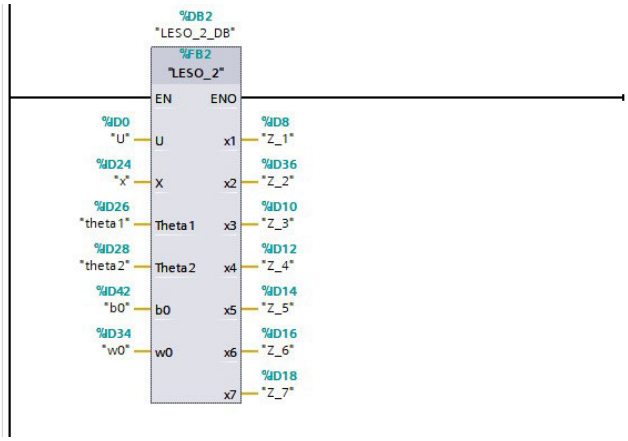

FIGURE 19. The LESO function block.

The PLC algorithm's flow chart is shown in Fig. 18. The OB1 organizational block is the main function, and its main function is cyclic waiting. The OB100 organizational block is system startup interruption, and interruption service function completes controller parameter assignment. The OB35 organizational block is a timing interruption. It realizes the interruption sequence every 100ms, completes sensor sampling in its interruption function, calculates the algorithm, updates the data, and sends back the control quantity to the motor driver, thus controlling the trolley motion in real-time.

The LESO is the core of LADRC. The PLC implementation process of the discrete LESO is described in detail. Because the implementation process is similar, the PD control law and the implementation process of the discrete TD will not be repeated.

The LESO module inputs are the control amount u and the real-time flat output X of the system, and the estimated values of each state and total disturbance of the system are z1, z2, z3, z4, z5, z6, z7, the output. For debugging purposes, the controller bandwidth w0 is used as its external input.

Complete the data transfer from k +1 to k with MOV instructions, then run the program based on k-cycle, calculate the next cycle's results, save again, implement the algorithm, and data update. To ensure the algorithm's discrete accuracy, the discrete LADRC algorithm is implemented using the cyclic break block OB35 with a break time of 100ms.

The function block of the discrete LESO is shown in Fig.19.

ACKNOWLEDGMENT

The authors are very grateful for the insightful comments and suggestions from the Associate Editor and all reviewers, which are very helpful to improve the quality of this article.

REFERENCES

[1] K. T. Hong, C. D. Huh, and K.-S. Hong, "Command shaping control for limiting the transient sway angle of crane systems," *Int. J. Control Autom. Syst.*, vol. 1, no. 1, pp. 43–53, Mar. 2003.

[2] H. I. Jaafar, S. Y. S. Hussien, R. Ghazali, and Z. Mohamed, "Optimal tuning of PID+PD controller by PFS for gantry crane system," in *Proc. 10th Asian Control Conf. (ASCC)*, May/Jun. 2015, pp. 1–6, doi: 10.1109/ASCC.2015.7244695.

[3] L. Ramli, Z. Mohamed, A. M. Abdullahi, H. I. Jaafar, and I. M. Lazim, "Control strategies for crane systems: A comprehensive review," *Mech. Syst. Signal Process.*, vol. 95, pp. 1–23, Oct. 2017, doi: 10.1016/j.ymssp.2017.03.015.

[4] L. Ramli, Z. Mohamed, and H. I. Jaafar, "A neural network-based input shaping for swing suppression of an overhead crane under payload hoisting and mass variations," *Mech. Syst. Signal Process.*, vol. 107, pp. 484–501, Jul. 2018, doi: 10.1016/j.ymssp.2018.01.029.

[5] J. J. Potter and W. E. Singhose, "Design and human-in-the-loop testing of reduced-modification input shapers," *IEEE Trans. Control Syst. Technol.*, vol. 24, no. 4, pp. 1513–1520, Jul. 2016, doi: 10.1109/TCST.2015.2487858.

[6] X. Xie, J. Huang, and Z. Liang, "Using continuous function to generate shaped command for vibration reduction," *Proc. Inst. Mech. Eng., I, J. Syst. Control Eng.*, vol. 227, no. 6, pp. 523–528, Jul. 2013, doi: 10.1177/0959651813488282.

[7] W. Singhose and J. Vaughan, "Reducing vibration by digital filtering and input shaping," *IEEE Trans. Control Syst. Technol.*, vol. 19, no. 6, pp. 1410–1420, Nov. 2011, doi: 10.1109/TCST.2010.2093135.

[8] N. Sun, Y. Fang, and X. Zhang, "Energy coupling output feedback control of 4-DOF underactuated cranes with saturated inputs," *Automatica*, vol. 49, no. 5, pp. 1318–1325, May 2013, doi: 10.1016/j.automatica.2013.01.039.

[9] N. Sun and Y. Fang, "New energy analytical results for the regulation of underactuated overhead cranes: An end-effector motion-based approach," *IEEE Trans. Ind. Electron.*, vol. 59, no. 12, pp. 4723–4734, Dec. 2012, doi: 10.1109/TIE.2012.2183837.

[10] K. Nakazono, K. Ohnishi, H. Kinjo, and T. Yamamoto, "Load swing suppression for rotary crane system using direct gradient descent controller optimized by genetic algorithm," *Trans. Inst. Syst., Control Inf. Eng.*, vol. 22, no. 8, pp. 303–310, Apr. 2009, doi: 10.5687/iscie.22.303.

[11] Y. Fang, B. Ma, P. Wang, and X. Zhang, "A motion planning-based adaptive control method for an underactuated crane system," *IEEE Trans. Control Syst. Technol.*, vol. 20, no. 1, pp. 241–248, Jan. 2012, doi: 10.1109/TCST.2011.2107910.

[12] N. Sun, X. Zhang, Y. Fang, and Y. Yuan, "Transportation task-oriented trajectory planning for underactuated overhead cranes using geometric analysis," *IET Control Theory Appl.*, vol. 6, no. 10, pp. 1410–1423, Jul. 2012, doi: 10.1049/iet-cta.2011.0587.

[13] K. Alghanim, A. Mohammed, and M. T. Andani, "An input shaping control scheme with application on overhead cranes," *Int. J. Nonlinear Sci. Numer. Simul.*, vol. 20, no. 5, pp. 561–573, Aug. 2019, doi: 10.1515/ijnsns-2018-0152.

[14] D. Liu and W. Guo, "GA-based stable intelligent control for a class of underactuated mechanical systems," *Int. J. Appl. Electromagn. Mech.*, vol. 36, nos. 1–2, pp. 49–61, May 2011, doi: 10.3233/JAE-2011-1343.

[15] K. L. Sorensen, W. Singhose, and S. Dickerson, "A controller enabling precise positioning and sway reduction in bridge and gantry cranes," *Control Eng. Pract.*, vol. 15, no. 7, pp. 825–837, Jul. 2007, doi: 10.1016/j.conengprac.2006.03.005.

[16] Z. Wu and X. Xia, "Optimal motion planning for overhead cranes," *IET Control Theory Appl.*, vol. 8, no. 17, pp. 1833–1842, Nov. 2014, doi: 10.1049/iet-cta.2014.0069.

[17] M. Zhang, Y. Zhang, and X. Cheng, "An enhanced coupling PD with sliding mode control method for underactuated double-pendulum overhead crane systems," *Int. J. Control, Automat. Syst.*, vol. 17, no. 6, pp. 1579–1588, May 2019, doi: 10.1007/s12555-018-0646-0.

[18] B. Lu, Y. Fang, and N. Sun, "Continuous sliding mode control strategy for a class of nonlinear underactuated systems," *IEEE Trans. Autom. Control*, vol. 63, no. 10, pp. 3471–3478, Oct. 2018, doi: 10.1109/TAC.2018.2794885.

[19] L. A. Tuan and S.-G. Lee, "Sliding mode controls of double-pendulum crane systems," *J. Mech. Sci. Technol.*, vol. 27, no. 6, pp. 1863–1873, Jul. 2013, doi: 10.1007/s12206-013-0437-8.

[20] N. Sun, Y. Fang, H. Chen, Y. Fu, and B. Lu, "Nonlinear stabilizing control for ship-mounted cranes with ship roll and heave movements: Design, analysis, and experiments," *IEEE Trans. Syst., Man, Cybern. Syst.*, vol. 48, no. 10, pp. 1781–1793, Oct. 2018, doi: 10.1109/TSMC.2017.2700393.

[21] N. Sun, Y. Fang, H. Chen, and B. Lu, "Amplitude-saturated nonlinear output feedback antiswing control for underactuated cranes with double-pendulum cargo dynamics," *IEEE Trans. Ind. Electron.*, vol. 64, no. 3, pp. 2135–2146, Mar. 2017, doi: 10.1109/TIE.2016.2623258.

[22] N. Sun, T. Yang, H. Chen, Y. Fang, and Y. Qian, "Adaptive anti-swing and positioning control for 4-DOF rotary cranes subject to uncertain/unknown parameters with hardware experiments," *IEEE Trans. Syst., Man, Cybern. Syst.*, vol. 49, no. 7, pp. 1309–1321, Jul. 2019, doi: 10.1109/TSMC.2017.2765183.

[23] W. He, R. Ortega, J. E. Machado, and S. Li, "An adaptive passivity-based controller of a buck-boost converter with a constant power load," *Asian J. Control*, vol. 21, no. 1, pp. 581–595, Feb. 2019, doi: 10.1002/asjc.1751.

[24] X. Yang, S. S. Ge, and J. Liu, "Dynamics and noncollocated model-free position control for a space robot with multi-link flexible manipulators," *Asian J. Control*, vol. 21, no. 2, pp. 714–724, Mar. 2019, doi: 10.1002/asjc.1772.

[25] M. J. Maghsoudi, Z. Mohamed, A. R. Husain, and M. O. Tokhi, "An optimal performance control scheme for a 3D crane," *Mech. Syst. Signal Process.*, vols. 66–67, pp. 756–768, Jan. 2016, doi: 10.1016/j.ymssp.2015.05.020.

[26] H. Chen, Y. Fang, and N. Sun, "Optimal trajectory planning and tracking control method for overhead cranes," *IET Control Theory Appl.*, vol. 10, no. 6, pp. 692–699, Apr. 2016, doi: 10.1049/iet-cta.2015.0809.

[27] Y. Qian, Y. Fang, and B. Lu, "Adaptive repetitive learning control for an offshore boom crane," *Automatica*, vol. 82, pp. 21–28, Aug. 2017, doi: 10.1016/j.automatica.2017.04.003.

[28] Y. Qian and Y. Fang, "Switching logic-based nonlinear feedback control of offshore ship-mounted tower cranes: A disturbance observer-based approach," *IEEE Trans. Autom. Sci. Eng.*, vol. 16, no. 3, pp. 1125–1136, Jul. 2019, doi: 10.1109/TASE.2018.2872621.

[29] K. A. Alghanim, K. A. Alhazza, and Z. N. Masoud, "Discrete-time command profile for simultaneous travel and hoist maneuvers of overhead cranes," *J. Sound Vibrat.*, vol. 345, pp. 47–57, Jun. 2015, doi: 10.1016/j.jsv.2015.01.042.

[30] N. Sun and Y. Fang, "An efficient online trajectory generating method for underactuated crane systems," *Int. J. Robust Nonlinear Control*, vol. 24, no. 11, pp. 1653–1663, Jul. 2014, doi: 10.1002/rnc.2953.

[31] H. Ouyang, G. Zhang, L. Mei, X. Deng, and D. Wang, "Load vibration reduction in rotary cranes using robust two-degree-of-freedom control approach," *Adv. Mech. Eng.*, vol. 8, no. 3, pp. 1–11, Mar. 2016, doi: 10.1177/1687814016641819.

[32] Z. Wu, X. Xia, and B. Zhu, "Model predictive control for improving operational efficiency of overhead cranes," *Nonlinear Dyn.*, vol. 79, no. 4, pp. 2639–2657, Mar. 2015, doi: 10.1007/s11071-014-1837-8.

[33] X. Wu and X. He, "Enhanced damping-based anti-swing control method for underactuated overhead cranes," *IET Control Theory Appl.*, vol. 9, no. 12, pp. 1893–1900, Aug. 2015, doi: 10.1049/iet-cta.2014.1353.

[34] N. Sun, Y. Wu, Y. Fang, and H. Chen, "Nonlinear antiswing control for crane systems with double-pendulum swing effects and uncertain parameters: Design and experiments," *IEEE Trans. Autom. Sci. Eng.*, vol. 15, no. 3, pp. 1413–1422, Jul. 2018, doi: 10.1109/TASE.2017.2723539.

[35] N. Sun, Y. Fang, Y. Wu, and H. Chen, "Adaptive positioning and swing suppression control of underactuated cranes exhibiting double-pendulum dynamics: Theory and experimentation," in *Proc. 31st Youth Academic Annu. Conf. Chin. Assoc. Autom. (YAC)*, Nov. 2016, pp. 87–92, doi: 10.1109/YAC.2016.7804870.

[36] H. Ouyang, Z. Tian, L. Yu, and G. Zhang, "Adaptive tracking controller design for double-pendulum tower cranes," *Mechanism Mach. Theory*, vol. 153, Nov. 2020, Art. no. 103980, doi: 10.1016/j.mechmachtheory.2020.103980.

[37] M. Zhang, Y. Zhang, H. Ouyang, C. Ma, and X. Cheng, "Adaptive integral sliding mode control with payload sway reduction for 4-DOF tower crane systems," *Nonlinear Dyn.*, vol. 99, no. 4, pp. 2727–2741, Jan. 2020, doi: 10.1007/s11071-020-05471-3.

[38] H. Chen and N. Sun, "Nonlinear control of underactuated systems subject to both actuated and unactuated state constraints with experimental verification," *IEEE Trans. Ind. Electron.*, vol. 67, no. 9, pp. 7702–7714, Sep. 2020, doi: 10.1109/TIE.2019.2946541.

[39] H. Chen and N. Sun, "An output feedback approach for regulation of 5-DOF offshore cranes with ship yaw and roll perturbations," *IEEE Trans. Ind. Electron.*, early access, Feb. 2, 2021, doi: 10.1109/tie.2021.3055159.

[40] T. Yang, N. Sun, Y. Fang, X. Xin, and H. Chen, "New adaptive control methods for n-link robot manipulators with online gravity compensation: Design and experiments," *IEEE Trans. Ind. Electron.*, early access, Jan. 14, 2021, doi: 10.1109/tie.2021.3050371.

[41] T. Yang, N. Sun, and Y. Fang, "Adaptive fuzzy control for a class of MIMO underactuated systems with plant uncertainties and actuator deadzones: Design and experiments," *IEEE Trans. Cybern.*, early access, Feb. 2, 2021, doi: 10.1109/TCYB.2021.3050475.

[42] Z. Gao, "Scaling and bandwidth-parameterization based controller tuning," in *Proc. Amer. Control Conf.*, vol. 6, Jun. 2003, pp. 4989–4996, doi: 10.1109/acc.2003.1242516.

[43] J. Han, "Active disturbance rejection control," in *Active Disturbance Rejection Control Technique-the Technique for Estimating and Compensating the Uncertainties*, Beijing, China: National Defense Industry Press, 2008, pp. 243–288.

[44] J. Chen, J. Wang, Y. Liu, and Z. Hu, "Design and verification of aero-engine rotor speed controller based on U-LADRC," *Math. Problems Eng.*, vol. 2020, pp. 1–12, May 2020, doi: 10.1155/2020/6798492.

[45] C. Liu, G. Luo, X. Duan, Z. Chen, Z. Zhang, and C. Qiu, "Adaptive LADRC-based disturbance rejection method for electromechanical servo system," *IEEE Trans. Ind. Appl.*, vol. 56, no. 1, pp. 876–889, Jan. 2020, doi: 10.1109/TIA.2019.2955664.

[46] L. Yu, R. Wang, W. Xia, and W. Wang, "An anti-windup method for a class of uncertain MIMO systems subject to actuator saturation with LADRC," *Inf. Sci.*, vol. 462, pp. 417–429, Sep. 2018, doi: 10.1016/j.ins.2018.06.039.

[47] C. Liu, G. Luo, Z. Chen, and W. Tu, "Measurement delay compensated LADRC based current controller design for PMSM drives with a simple parameter tuning method," *ISA Trans.*, vol. 101, pp. 482–492, Jun. 2020, doi: 10.1016/j.isatra.2020.01.027.

[48] Y. W. Wang, W. A. Zhang, H. Dong, and L. Yu, "A LADRC based fuzzy PID approach to contour error control of networked motion control system with time-varying delays," *Asian J. Control*, vol. 22, no. 5, pp. 1973–1985, Apr. 2020, doi: 10.1002/asjc.2080.

[49] C. Li, X. Zhou, Y. Ma, and L. Shao, "The LADRC control system of distribution static synchronous compensator based on chaotic sequences PFPWM," *Adv. Sci. Lett.*, vol. 11, no. 1, pp. 556–560, May 2012, doi: 10.1166/asl.2012.2966.

[50] C. Liu, Y. Cheng, D. Liu, G. Cao, and I. Lee, "Research on a LADRC strategy for trajectory tracking control of delta high-speed parallel robots," *Math. Problems Eng.*, vol. 2020, pp. 1–12, Aug. 2020, doi: 10.1155/2020/9681530.

[51] M. Fliess, J. Lévine, P. Martin, and P. Rouchon, "Flatness and defect of non-linear systems: Introductory theory and examples," *Int. J. Control*, vol. 61, no. 6, pp. 1327–1361, Jun. 1995, doi: 10.1080/00207179508921959.

[52] J. Han, "From PID to active disturbance rejection control," *IEEE Trans. Ind. Electron.*, vol. 56, no. 3, pp. 900–906, Mar. 2009, doi: 10.1109/TIE.2008.2011621.

[53] Z. Gao, "Active disturbance rejection control: From an enduring idea to an emerging technology," in *Proc. 10th Int. Workshop Robot Motion Control (RoMoCo)*, Jul. 2015, pp. 269–282, doi: 10.1109/RoMoCo.2015.7219747.

[54] B.-Z. Guo and H.-C. Zhou, "The active disturbance rejection control to stabilization for multi-dimensional wave equation with boundary control matched disturbance," *IEEE Trans. Autom. Control*, vol. 60, no. 1, pp. 143–157, Jan. 2015, doi: 10.1109/TAC.2014.2335511.

[55] C. Huang, B. Du, and Q. Zheng, "Design and Implementation of PLC Based Linear Active Disturbance Rejection Control Approach," *Control Eng. China.*, vol. 24, no. 1, pp. 171–177, 2017.

[56] X.-B. Meng, X. Z. Gao, L. Lu, Y. Liu, and H. Zhang, "A new bio-inspired optimisation algorithm: Bird swarm algorithm," *J. Exp. Theor. Artif. Intell.*, vol. 28, no. 4, pp. 673–687, Jul. 2016, doi: 10.1080/0952813X.2015.1042530.

[57] D. Zhang, J. Yang, and P. Yang, "An improved chaos bird swarm optimization algorithm," in *Proc. J. Phys., Conf.*, Mar. 2019, vol. 1176, no. 2, Art. no. 022016, doi: 10.1088/1742-6596/1176/2/022016.

[58] H. Yang, T. Chen, and N.-J. Huang, "An adaptive bird swarm algorithm with irregular random flight and its application," *J. Comput. Sci.*, vol. 35, pp. 57–65, Jul. 2019, doi: 10.1016/j.jocs.2019.06.004.

[59] L. Chai and H. Liu, "Design of crane anti-swing controller based on differential flat and linear active disturbance rejection control," in *Proc. 6th Int. Conf. Syst. Informat. (ICSAI)*, Nov. 2019, pp. 81–85, doi: 10.1109/ICSAI48974.2019.9010558.

[60] N. Sun, Y. C. Fang, and Y. Z. Qian, "Motion planning for cranes with double pendulum effects subject to state constraints," *Kongzhi Lilun Yu Yingyong/Control Theory Appl.*, vol. 31, no. 7, pp. 974–980, Jul. 2014, doi: 10.7641/CTA.2014.40054.

LIN CHAI received the M.Eng. and Ph.D. degrees from the Wuhan University of Science and Technology, Wuhan, China, in 2005 and 2019, respectively. Since 2005, he has been with the College of Information Science and Engineering, Wuhan University of Science and Technology, where he is currently an Associate Professor. He has published more than ten papers in journals and international conferences. His major research interests include under-actuated system control, intelligent control, industrial network control, power systems, and its automation.

QIHANG GUO (Graduate Student Member, IEEE) received the B.Eng. degree from the Wuhan University of Science and Technology, Wuhan, China, in 2018, where he is currently pursuing the M.S. degree with the College of Information Science and Engineering. His research interest includes under-actuated system control.

HUIKANG LIU received the M.Eng. degree from the Wuhan University of Science and Technology, Wuhan, China, in 1988. Since 1988, he has been with the College of Information Science and Engineering, Wuhan University of Science and Technology, where he is currently a Professor. His major research interests include intelligent equipment, new electric drive, and equipment fault diagnosis.

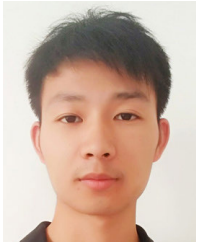

MINGBO DING received the B.Eng. degree from the Hubei University of Automotive Technology, Hubei, China, in 2019. He is currently pursuing the M.S. degree with the College of Information Science and Engineering, Wuhan University of Science and Technology, Wuhan, China. His research interest includes under-actuated system control.